Microchemical Journal 205 (2024) 111257

Contents lists available at ScienceDirect

Microchemical Journal

journal homepage: www.elsevier.com/locate/microc

Design of blue-emitting adenosine monophosphate-copper nanocluster: Detection of Vitamin B_2 in real samples

Ditta Ungor [a,b,*], Loretta Kuklis [a], Gergely F. Samu [b,c], Edit Csapó [a,b]

[a] MTA-SZTE Lendület "Momentum" Noble Metal Nanostructures Research Group, University of Szeged, Rerrich B. sqr. 1, H-6720 Szeged, Hungary
[b] Interdisciplinary Excellence Center, Department of Physical Chemistry and Materials Science, University of Szeged, Rerrich B. sqr. 1, H-6720 Szeged, Hungary
[c] Department of Molecular and Analytical Chemistry, University of Szeged, Dóm Square 7-8, H-6721 Szeged, Hungary

ARTICLE INFO

Keywords:
Blue emission
Cu
Riboflavin
Dynamic quenching
Yeast
Pills

ABSTRACT

We demonstrate a simple preparation protocol for the synthesis of novel adenosine monophosphate-stabilized copper nanoclusters (AMP-Cu NCs). Synthesis parameters are optimized to reach the best fluorometric signal. The prepared Cu NCs show characteristic blue emission at 430 nm, which is related to the presence of Cu_{13} metal cores. Three distinct lifetime components are identified and the metallic feature of the NCs is proven by X-ray photoelectron spectroscopy. The stability and the long-term storage of the AMP-Cu NCs were investigated by pH- and time-dependent measurements. Besides the synthesis and characterization, a possible liquid fluorescent assay method is also developed for the detection of the biologically important Vitamin B_2 in complex real samples by with 2.01 ± 0.31 μM detection limit. For the real samples, the yeast and dietary supplements were selected, where the detected concentration of Riboflavin was in good agreement with the expected amount in these complex chemical systems.

1. Introduction

One of the major challenges nowadays is the development of novel and ultrasensitive (bio)sensing platforms to detect several biologically important or harmful molecules in real samples. These new techniques can offer to replace expensive and specific measurement procedures, but they must also fulfill several criteria at the same time. From the synthesis side, the raw materials should be eco-friendly and cheap, and the preparation protocols need to be easily implementable and cost-effective. Fluorescent noble metal nanoclusters (NCs) became increasingly relevant materials in the last ten years [1–3] because these ultrasmall particles, which are composed from only a few or a several number of atoms, can overcome the above-mentioned challenges. They have unique size- and composition-dependent optical features [4] and various biomolecules [5,6] can be applied for their synthesis. Therefore, their expected characteristics can be easily tuned towards future applications.

In the last few years, the possible application of fluorescent noble metals in food-related chemistry for the detection of harmful ions [7,8], toxins [8–10], or other molecules [11–13] was explored. For example, Y. Shi and co-workers developed a bimetallic Cu/Au NCs-based aptasensor for the detection of harmful Hg^{2+} ions in seaweed samples with a 4.92 nM limit of detection (LOD) [14]. In the work of L. Chen, an ultrasensitive sensing platform from nitrogen-doped carbon dots and Cu NCs was developed, which is suitable for the identification of pesticides (thiram and paraquat) in lotus seeds, millet, and ginseng [15]. To the best of our knowledge, the potential sensor applications of noble metal NCs related to the Vitamin B molecular family mostly focus on the detection of B_9 (folic acid) in solutions and HeLa cells [16–18]. For the identification of other Vitamin B derivatives, only a few examples exist in the literature [17,19,20]. In our previous study, a possible measurement method for the detection of folic acid in aqueous solutions by adenosine monophosphate (AMP)-stabilized bimetallic Au/Ag NCs [21] was presented. Moreover, a paper-based drop test was also developed as a step towards future application as rapid assay in biomedical fields.

For the sensor application of the fluorescent NCs, AMP as the stabilizing ligand can be an excellent candidate due to its several functional N-containing groups for the primer coordination of noble metal ions. One of the first works by A. Lopez and J. Liu focuses on the potential application of the adenine derivates for the preparations of gold-based fluorescent supramolecular complexes [22]. Their original work facilitated the use of smaller building block molecules as ligands in addition

* Corresponding author at: MTA-SZTE Lendület "Momentum" Noble Metal Nanostructures Research Group, University of Szeged, Rerrich B. sqr. 1, H-6720 Szeged, Hungary.
E-mail address: ungord@chem.u-szeged.hu (D. Ungor).

https://doi.org/10.1016/j.microc.2024.111257
Received 23 February 2024; Received in revised form 17 July 2024; Accepted 19 July 2024
Available online 20 July 2024
0026-265X/© 2024 Elsevier B.V. All rights are reserved, including those for text and data mining, AI training, and similar technologies.

to the traditional protein or polymer template-assisted syntheses. In the last decade, several other works [23,24] expanded the plethora of synthesis methods to prepare monometallic Au or bimetallic Au/Ag complexes and clusters with using AMP as a ligand. In contrast, copper, which is a potentially cost-effective and prominent raw material, has been neglected so far due to the well-known oxidation process in the nanometer size range [25]. Based on the literature data, the most popular and commonly used bottom-up synthesis technique in the case of copper-based NCs is template-assisted synthesis, which applies various peptides, DNA, and polymers [26,27]. Although the formation of copper-based complexes of the nitrogen and sulfur-containing small (bio)molecules has been well-known for decades [28,29], the synthesis of stable Cu NCs with amino acids or nucleotides is yet to be explored.

The main motivation of this work was to study the effect of metal exchange (from the Au/Ag to pure Cu) on the structural and optical characteristics, as well as the potential sensor application, of the AMP-functionalized NCs. We investigated the synthesis conditions to reach the highest yield and fluorescence magnitude. The photo- and colloid stability of the Cu-based system was revealed at different pH and ionic strength conditions. The long-term effect of UV-light exposure ($\lambda_{max,1}$ = 256 nm and $\lambda_{max,2}$ = 365 nm) on the emission features was also examined. Finally, a potential application avenue [30–32] as a rapid liquid fluorescent assay for the Vitamin B molecular family member Vitamin B_2 is also presented for food and pharmaceutical samples.

2. Materials and protocols

2.1. Chemicals

For the synthesis the adenosine 5′-monophosphate disodium salt ($C_{10}H_{12}N_5Na_2O_7P$, AMP; 99.0 %; Sigma), copper(II) chloride dihydrate ($CuCl_2{\cdot}2H_2O$; Sigma), citric acid monohydrate ($C_6H_8O_7{\cdot}H_2O$; 99.9 %; Molar), trisodium citrate dihydrate ($C_6H_5Na_3O_7{\cdot}2H_2O$; 99.9 %; Molar), sodium hydroxide (NaOH; 99.8 %; Molar) and hydrochloric acid (HCl; 37 %; Molar) were applied. During the sensor measurement, folic acid ($C_{19}H_{19}N_7O_6$; Vitamin B_9; ≥97.0 %; Sigma), calcium pantothenate ($C_9H_{16}NO_5$ × 1/2 Ca; Vitamin B_5; 98 %; Sigma), niacin (3-(COOH)-C_5H_4N; Vitamin B_3; 98 %, Sigma), riboflavin ($C_{17}H_{20}N_4O_6$; Vitamin B_2, ≥ 98.0 %; Sigma) and thiamine hydrochloride ($C_{12}H_{17}ClN_4OS{\cdot}HCl$; Vitamin B_1; ≥ 99 %; Sigma), sodium chloride (NaCl; 99.9 %; Molar) and potassium chloride (KCl; 99 %; Molar) were used. The reagents were applied without further purification due to their analytical grade. The stock solutions were prepared freshly with Milli-Q (Merck Millipore) ultrapure water (conductivity: 18.2 MΩ·cm). For the purification, the Pur-A-Lyzer™ dialysis kit (Sigma) having a 1 kDa cut-off value was chosen.

2.2. Synthesis of AMP-Cu NCs

During synthesis, AMP:Cu/10:1 M ratio was applied by using 5.0 mM and 0.5 mM final concentrations of AMP and Cu, respectively. Namely, 5 mL of AMP solution (c_{AMP}=0.2 M) was diluted with 154 mL of ultrapure water, then 2 mL of $CuCl_2$ solution (c_{CuCl2} = 0.1 M) was pipetted into the reaction mixture. After 5 min stirring at room temperature, 40 mL of 0.5 M citric acid/citrate buffer solution (pH=6.0) was added. The sample was thermostated at 80 °C for 29 days. After the synthesis, the purification was applied for 150 min with a manufactured Pur-A-Lyzer™ dialysis kit (cut-off: 1 kDa), where ultrapure water served as the dialysis medium. The final samples can be stored in the fridge at 4 °C for more than two months without any significant quality degradation.

2.3. Sensor measurements

During the liquid sensor measurements, the clusters were applied in *ca.* 0.1 mM concentration referring to the metal content. Each individual sample contains 1 mL purified AMP-Cu NCs, 0.15 M NaCl, and an adequate amount of riboflavin to reach of 2–1000 μM final concentration at pH=8.0. The studied concentration range was 0.1 nM–1 mM and after the measurements, the spectra were corrected for inner filter and self-absorption effects. The measurement of the real samples dietary supplements and yeast were selected. For the preparation, three packages having different production times were used in the case of each type. In every case, 5 pills were chosen from the boxes to create one datapoint. In the case of yeast, all three sets were divided into 5 parts, and then from these parts, the required amount were applied for the dissolution. In summary, 15 individual samples were analyzed from each real samples as followings in order to achieve a sampling matrix. For the stock solutions, 0.2 g yeast was dissolved directly in 20 mL ultrapure water (pH=8.0). The pills were crushed in an agate mortar, then 0.26 ± 0.01 g/pill was dissolved in 20 mL alkali water, as well. For the final measurements, the solutions of the pills were diluted 100-fold. The individual test samples contain 2 mL AMP-Cu NCs, 20 μL of 1 M NaOH to reach the aggregated form of the NCs and 200 μL of the yeast or pill solutions.

2.4. Instruments

The UV–Vis spectra were recorded with an ABL&E JASCO V-770 Spectrophotometer in a 1 cm standard quartz cuvette. For the measurements, the main settings were 200 nm/min scan speed, and 1 nm data interval in the 200–900 nm wavelength range. The HOMO-LUMO energy gap of the Cu NCs and Vitamin B_2 were calculated by the Tauc plot of the recorded spectra. For the studies of the fluorescence of the prepared NCs, steady-state and time-resolved measurements were used. The excitation and emission spectra were registered on the ABL&E JASCO FP-8500 spectrofluorometer using a 1 cm optical length. During the measurements, 2.5–2.5 nm bandwidth both in the excitation and emission directions, 200 nm/min scan speed, and 1 nm resolution were applied. The absolute internal quantum yield (QY %) was calculated based on the incident light spectra and the indirect and direct excitation of the samples in 2 mm optical length on the same apparatus equipped with the ABL&E JASCO ILF-835 integrating sphere. The instrument was calibrated by using ABL&E JASCO ESC-842 calibrated WI light source, thus, other references were not needed. For the calculations, the SpectraManager 2.0 software of the instrument was used. The fluorescence lifetime of AMP-Cu NCs was determined by time-correlated single photon counting (TCSPC) on a Horiba DeltaFlex device equipped with a DeltaDiode pulsed laser (λ_{laser} = 371 nm) in a 1 cm quartz cuvette. The emitted light was detected at 430 nm with a 4 nm slit. The number of counts on the peak channel was 10,000 and to determine the instrument response function (IRF), standard SiO_2 colloids Horiba) was applied. The main lifetime components were calculated in the EZTime program of Horiba by the exponential fitting of decay curves and the goodness of fitting was characterized by χ^2 values. To verify the cluster-type metallic structure of the prepared AMP-Cu NCs, XPS measurements were carried out. The spectra were registered on a SPECS instrument equipped with a PHOIBOS 150MCD9 hemispherical analyzer. For both the survey scan and transmission mode, 40 eV pass energy was selected. The sample was deposited by multistep cyclic freeze drying on a titanium foil having 0.5 mm thickness (Sigma). The Al Ka X-ray source was used at 200 W power. The 1 s peak of the carbon (284.80 eV) was used for charge referencing and the recorded spectra were evaluated by CasaXPS software. For the identification of the stabilizer moieties of AMP, Fourier-transformed Infrared spectroscopy (FT-IR) was applied, which was implemented on a JASCO FT/IR-4700 instrument. The device was equipped with an ATR PRO ONE single-reflection accessory and the spectra were recorded in the range of 500–4000 cm^{-1} with 1 cm^{-1} resolution based on 128 interferograms. The measurements were conducted on the lyophilized AMP-Cu NCs and the lyophilized AMP powders after the dissolution of the ligand at the same concentrations and similar pH to the cluster dispersions. The aggregation tendency of the fluorescent nano-objects was studied on a Malvern Zetasizer NanoZS ZEN 4003 apparatus

equipped with a He-Ne laser (λ = 633 nm) at 25 ± 0.1 °C and 0.1 M ionic strength by NaCl. For this purpose, the hydrodynamic diameters (d_H) and the ζ-potentials by the Smoluchowski model were measured. All samples were consecutively measured by five times. For cyclic voltammetry (CV), a Metrohm DropSense μStat 400 Bipotentiostat/Galvanostat was used. In the electrochemical cell, the Metrohm-manufactured screen-printed carbon electrode (SPCE) was used, where the working and counter electrode was a carbon film, and a AgCl-covered Ag electrode served as a reference electrode. The measurements were carried out in 0.1 M KCl aqueous solution which contains the AMP-Cu NCs suspension or the solution of Vitamin B_2 with a 50 mV/s sweep rate at 25 °C. The potential window was between −0.4 V and + 1.0 V.

3. Results & discussion

3.1. Synthesis of AMP-Cu NCs

First, the molar ratios of the components were varied between AMP:Cu/0.1:1–100:1, while the initial metal concentration was fixed at 1 mM. The temperature was kept at 40 °C during the syntheses. In the first few days, the optical changes were not significant. After 7 days, the initial intensive blue color of the $CuCl_2$ became fainter and a weak blue fluorescence appeared in the case of molar ratio > n_{AMP}:n_{Cu}/5:1 (Fig. S1A). The most intense fluorescence was developed at *10:1/AMP:Cu* ratio.

Previous studies pointed out that for the synthesis of noble metal-based fluorescent supramolecular structures, the *ca.* pH=6.0 value is preferable, which can be regulated by the citrate buffer solution. The buffer has a dual role during the synthesis: (i) it causes the total deprotonation of the appropriate coordination groups in the AMP molecule [22,33], (ii) the presence of citrate can help the total reduction of metal ions and the formation of the cluster structure. For this purpose, five citrate buffer solutions with different pH values (such as 3.0; 4.0; 5.0; 6.0, and 6.2) were used to find the ideal initial condition to reach the highest emission intensity. Based on the recorded spectra, a characteristic blue emission was identified at *ca.* 420–430 nm using 365 nm as the excitation wavelength. The formation of the fluorescent adduct is a slow process in the beginning, therefore the spectra were recorded after 7 days. Our results also confirm that the application of *pH=6.0* is the most advantageous (Fig. S1B) in terms of achieving high emission intensity.

Next, we explored the effect of the initial metal content for the synthesis. For this purpose, the c_{Cu} was varied between 0.1–10.0 mM in the individual samples at the beginning of the synthesis. It was found that after 14 days, the *0.5 mM* initial copper(II) ion concentration results in the best emission signal intensity (Fig. S2A). The use of higher concentrations already promoted the formation of larger aggregates and particles, therefore resulting in a weaker fluorescence signal in the sample. The effect of temperature was also investigated on the formed Cu-based systems. At 25 °C, no fluorescence signal can be detected even after 1 month, while at higher temperatures the formation of fluorescent adducts can be observed in the span of weeks. For achieving the best PL intensity, the synthesis should be carried out at *80 °C* (Fig. S2B). At this temperature, the total time for the controlled synthesis was *29 days* using the previously fixed ideal conditions (AMP:Cu^{2+}/10:1, c_{Cu}^{2+} = 0.5 mM, pH=6.0 by citrate buffer).

To remove any nonreacted copper salt and unnecessary additional materials, dialysis was applied for 150 min. After the purification, the Cu content of the clean sample was determined by mass spectrometry, which proved that the final concentration of Cu is *ca.* 0.46 mM. Therefore, the yield is more than 90 % related to the metal content.

3.2. Identification of the formed fluorescent nanocluster

The purified product was characterized in detail. The sample shows blue emission under a UV-lamp as shown in Fig. 1A. The measured excitation and emission maxima are at 370 and 425 nm, respectively, with a small Stoke shift, which refers to the formation of a metallic cluster-type structure. The identified wavelengths clearly belong to the Cu-based system because the surface AMP ligand has no characteristic optical signal in this region. The number of the atoms in the primer cluster cores can be calculated from the energy of the emission by Eq. (1) using the Jellium model [34] in the case of few-atomic noble metal NCs:

$$N = \left(\frac{E_{Fermi}}{E_{emission}}\right)^3 \quad (1)$$

where **N** is the number of atoms in the individual cores, $\mathbf{E_{Fermi}}$ and $\mathbf{E_{emission}}$ are the energies of the Fermi level of the bulk copper and the detected fluorescence, respectively. Based on the literature data, the E_{Fermi} is 7.0 eV in the case of the well-defined bulk Cu [35] therefore, the prepared sample contains *ca.* 13 Cu atoms in the primer metal cores [36], which can be stabilized by the formation of larger few-nanometer-sized particles.

To prove the few-atomic structure, time-dependent photoluminescence (PL) measurements were also carried out. Based on the

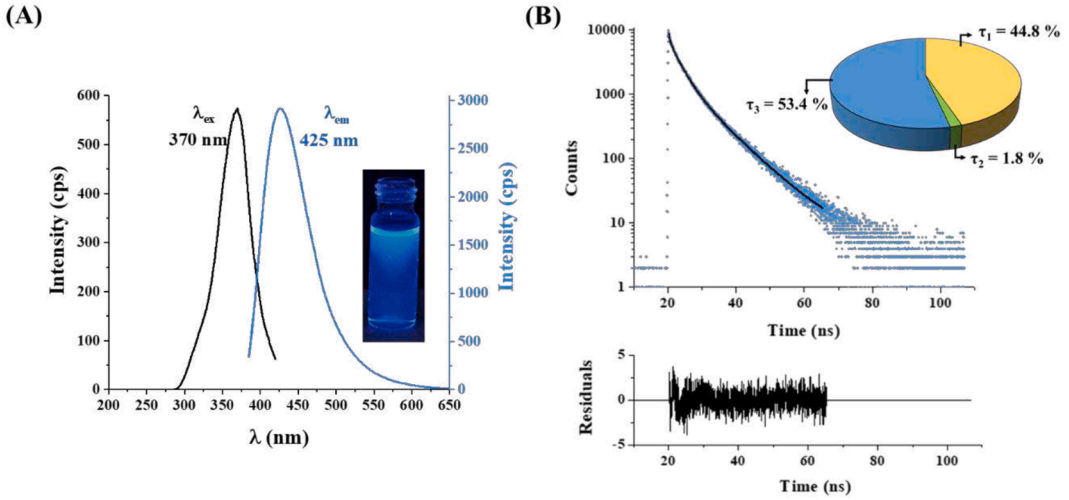

Fig. 1. (A) Excitation and emission spectra of the AMP-stabilized Cu nanoclusters with the photo of the sample under UV-lamp (c_{Cu} = 0.46 mM; $\lambda_{lamp,\ max}$ = 365 nm; T=25 °C). (B) The fluorescence decay profile with the fitting and the ratios of the estimated lifetime components, where the goodness of the fit is χ^2 = 1.09 (λ_{ex} = 371 nm; λ_{em} = 430 nm; T=25 °C).

decay curve (Fig. 1B), the average fluorescence lifetime (τ) is *ca.* 3.8 ns, which consists of three distinct components: $\tau_1 = 3.04 \pm 0.16$ ns (44.8 %), $\tau_2 = 0.31 \pm 0.06$ ns (1.8 %) and $\tau_3 = 8.72 \pm 0.13$ ns (53.4 %). The measured fluorescence parameters are in good agreement with the literature data [34]. The absolute internal QY % was calculated using an integrating sphere-equipped fluorometer, therefore any other dye references were not needed. The measured QY was 1.81 ± 0.27 %, which is a typical value for small biomolecule-stabilized noble metal quantum clusters [37].

The chemical composition of the prepared system was analyzed by XPS studies, where the presence of carbon, nitrogen, oxygen, sodium, and copper was identified in the survey scan (Fig. 2A) of the sample, while the titanium signal originates from the substrate.

Generally, the metallic Cu $2p_{3/2}$ peak is located at ~ 932.60 eV [38]. In the prepared sample, this peak appears at 933.02 eV (Fig. 2B), which shows a slightly positive shift due to the strong interaction with the ligand shell on the surface [39]. The absence of satellite features in the 940–950 eV regime confirms the presence of metallic Cu cores instead of Cu(I) [40]. The C 1 s core-level spectra (Fig. 2C), can be separated into three major components, belonging to the surface AMP molecules [41]. The N 1 s core-level spectrum consists of two major components (Fig. 2D). The peak at lower binding energy (399.3 eV) is attributed to the imine nitrogen, and the shoulder at higher binding energy at 400.9 eV can be assigned to the amine nitrogen [42].

For further verification of the binding between AMP and Cu, FT-IR spectra were registered. Fig. 3A proves the metallic feature of the Cu NCs because the intensity of the vibrations changes due to the difference in the selection rules. Among the coordination-capable moieties of the AMP, the N atoms show generally the highest affinity toward soft metals [43]. In the NCs, the formed metal cores are stabilized through the nitrogen-rich adenine ring based on the dominant shift of the N-content functional group vibrations. Namely, the stretching (ν) of the pyrimidine ring, (C_5-N_7), (N_1-C_2), (C_8-N_9), and (N_9-H) groups with the bending (β) of (C_8-H) moiety moves from 1351 cm^{-1} to 1397 cm^{-1}.

The stability of the AMP-Cu NCs was studied under different conditions. The hydrodynamic diameter (d_H), the ζ-potential, as well as the fluorescence intensity were measured at the same time (Fig. 3B). The NCs form smaller aggregates under highly acidic (pH~1.0) and alkaline (pH~12.0) conditions, which show weak luminescence due to the charge-shielding effect in high ionic strength media. In the mildly acidic region, individual sub-nanometer-sized cores can be identified with 0.6–0.9 nm average sizes and poor stability because the ζ-potentials are close to zero. After pH=6.0, the average d_H of the Cu NCs shows continuous growth until pH=8.0, while the PL intensity also increases due to the aggregation-induced emission process. Besides, the stability is also improved by the *ca.* −25 mV value of electrokinetic potential. It can be concluded that the small aggregates contain loose clumps of the metal cores, while the NCs fit tightly in the larger adducts between pH=7.0–10.0, by which the flexibility is decreased and the relaxation can be realized exclusively by the photoemission [44]. To examine the effect of high ionic strength, sodium chloride as inert salt was added to the cluster suspension. Based on the unchanged d_H values and fluorescence intensities, it can be concluded that the Cu NCs are stable even at 5 M NaCl concentration

To examine the photostability of the samples, 24 h of UV-light exposure was applied. For this purpose, two samples of 10 mL NCs suspension in quartz cuvette were stored under 15 W 254 nm and 365 nm UV irradiation for 7 days. Based on the registered spectra, the hard UV can degrade the AMP-Cu NCs within 3 days, but under mild UV irradiation the emission intensity of the nanoclusters is retained during the measurement window (Fig. S3A). Besides, the examination of the long-term storage possibility, the freeze-drying serves a suitable option because the re-dissolved suspension shows similar optical characteristics like the freshly prepared NCs (Fig. S3B). The recommended interval is 4 months without significant quality deterioration.

3.3. *Identification of Vitamin B_2 by fluorescence quenching of blue-emitting Cu NCs*

Considering our previous results [21], the changing the metal core in the AMP-stabilized metal NCs was investigated on the possible tuning of the selectivity for the Vitamin B molecular family (Fig. 4A). During the

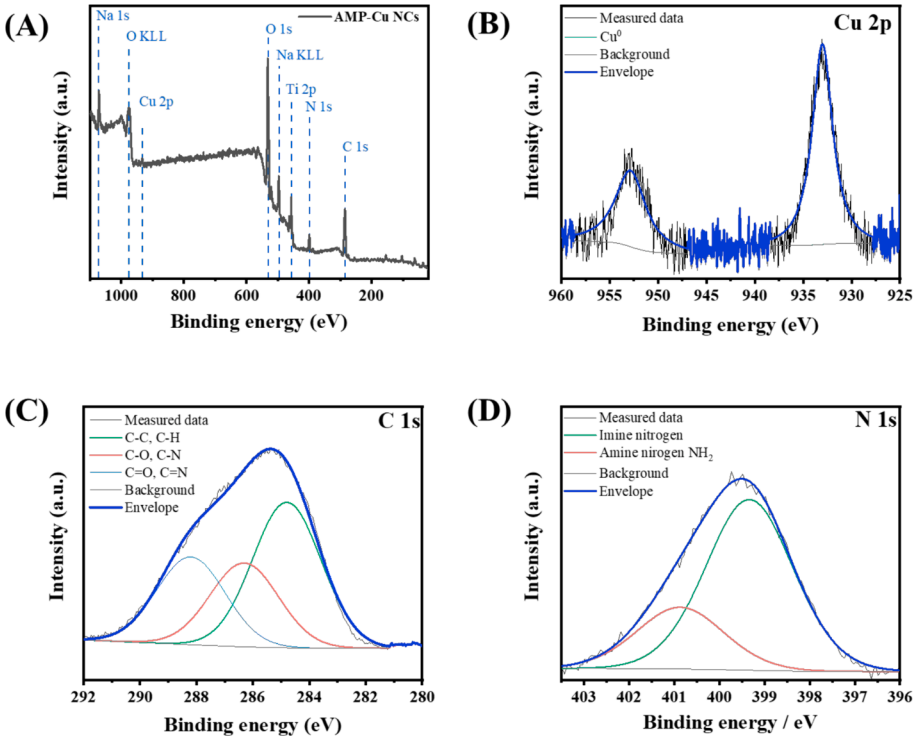

Fig. 2. (A) The survey scan and the high-resolution core level XPS spectra of the (B) Cu 2p, (C) C 1 s, and (D) N 1 s of the AMP-Cu NCs.

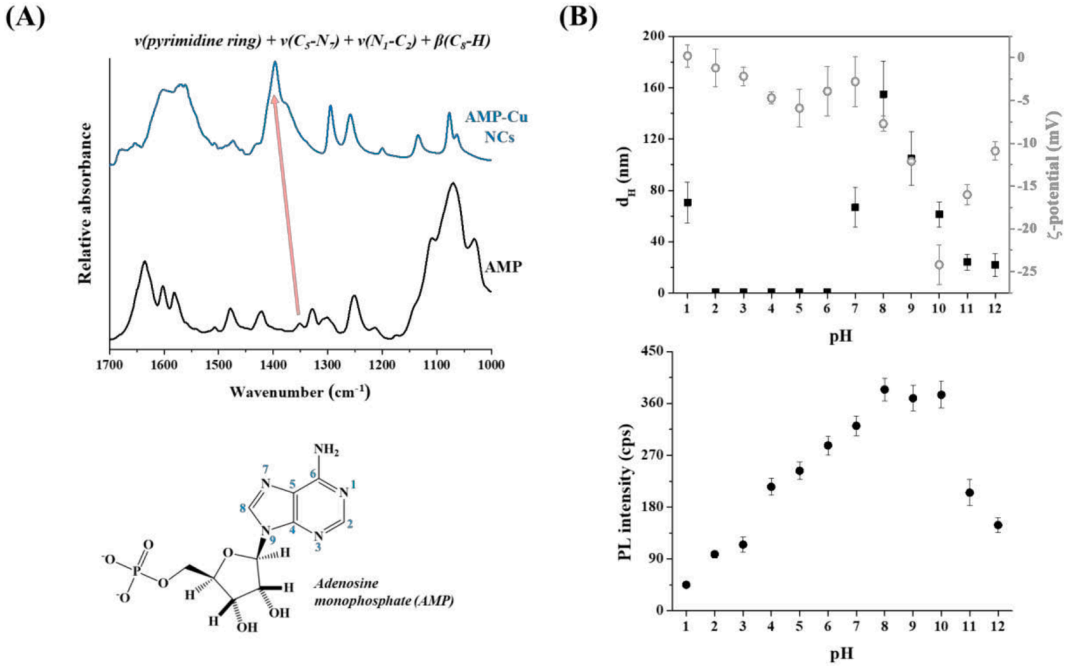

Fig. 3. (A) The FT-IR spectra of AMP-Cu NCs and pure AMP. (B) The measured d_H (■) and ζ-potential values (○) with the maxima of emission (●) of the samples depending on the applied pH (T=25 °C; I=0.1 M of NaCl). Error bars represent the standard deviation of measurements on three different individual samples.

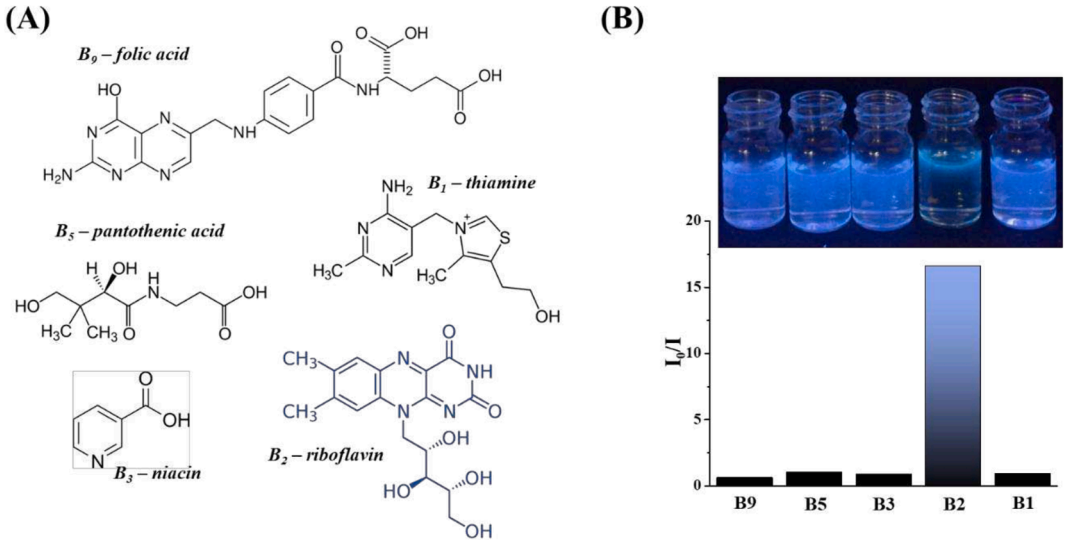

Fig. 4. (A) The chemical structures of the studied Vitamin B molecules. (B) The relative fluorescence (I_0/I) and the photos of the samples under UV-lamp ($\lambda_{lamp,\ max}$ = 365 nm) after the addition of 5 μM of different B Vitamins.

measurements, individual samples were prepared using 0.15 M of NaCl solutions at pH=8.0 to keep the ionic strength constant and promote the dissolution of the molecules. As Fig. 4B shows, dominant fluorescence quenching can be observed only after the addition of riboflavin (Vitamin B_2).

For better understanding the quenching process, a deeper investigation of the Cu NCs/B_2 complex system was needed because the polynomial behavior of an order 2 refers to a complex quenching mechanism. For this purpose, the τ of the Cu NCs was measured with the absence and presence of B_2. As can be seen on Fig. 5A, the average τ is decreased by *ca.* 50 % after the addition of Vitamin B_2, which refers to a dominant dynamic quenching. Considering the large spectral overlap of the absorbance of riboflavin and the excitation/emission of the Cu NCs (Fig. 5B), it can be concluded that the quenching is realized via resonance energy transfer (RET).

For further analysis, electrochemical measurements were carried out. Based on the recorded voltammogram of AMP-Cu NCs (Fig. 5C), the prepared Cu NCs have two dominant oxidation peaks at 0.450 and 0.860 V referring to a two-step oxidation process of the metallic seeds. The HOMO energy of the AMP-Cu NCs was calculated by Eq. (2):

$$E_{HOMO} = -(E'_{onset} + 4.4)eV \quad (2)$$

where the $\mathbf{E'_{onset}}$ was the onset potential of the first oxidation process. The measured E'_{onset} is 0.330 V vs Ag/AgCl pseudoreference electrode, which is equal to 0.618 V vs normal hydrogen electrode. The measured E_{onset} is in good agreement with the $E_{Cu(I)/Cu}$ (0.52 V), which strongly depends on the coordination sphere of the copper atoms [45]. For the calculation 0.618 V were used, therefore, the E_{HOMO} is −5.02 eV in the

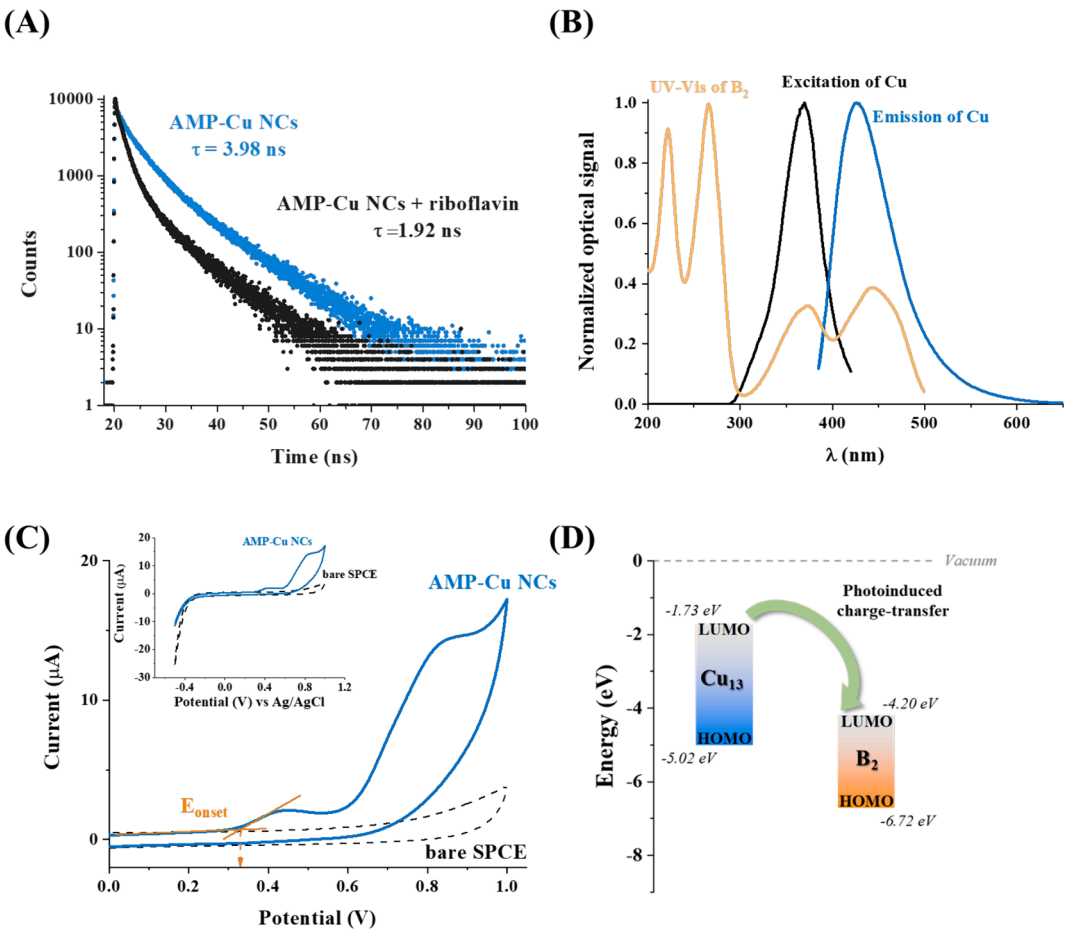

Fig. 5. (A) The fluorescence decay curves with the average lifetime values of AMP-Cu NCs before and after the addition of Vitamin B_2 (λ_{ex} = 371 nm; λ_{em} = 430 nm; c_{Cu} = 0.1 mM; T=25 °C; pH=8.0; c_{NaCl} = 0.15 M). (B) The normalized UV–Vis spectra (Vitamin B_2) and emission/excitation spectra (AMP-Cu NCs). (C) Cyclic voltammograms of the AMP-Cu NCs in 0.1 M KCl with Ag/AgCl reference electrode. (D) The schematic diagram of the HOMO-LUMO energy levels of AMP-Cu NCs and Vitamin B_2.

case of AMP-Cu NCs.

In the absence of reduction peak(s) on the CV, the energy level of the LUMO can be calculated by the HOMO-LUMO energy gap ($\mathbf{E_g}$). For the calculation, the Tauc plot of the registered UV–Vis spectrum (Fig. S4) was used, which clearly show that the E_g is 3.29 eV of the prepared AMP-Cu NCs. Using the $\mathbf{E_g = E_{LUMO}\text{-}E_{HOMO}}$ relation [46], the E_{LUMO} is −1.73 eV. Based on the literature data of the energy levels of Vitamin B_2 [47], it can be concluded that the possible photoinduced charge-transfer can be realized between the AMP-Cu NCs and Vitamin B_2 during the quenching process (Fig. 5D), which results a reduced form (Fig. S5) [48] of riboflavin.

For the possible sensor application, the inner filter effect was eliminated by Eq. (3):

$$I_c = I_m \times 10^{(A_{EX}+A_{EM})/2} \quad (3)$$

where, the $\mathbf{I_c}$ and $\mathbf{I_m}$ are the corrected and the measured intensities at 425 nm, respectively. The $\mathbf{A_{EX}}$ and $\mathbf{A_{EM}}$ are the absorbance at the excitation and emission wavelengths.

Although the emission of NCs is inhibited by the B_2 in the whole concentration range, the limit of detection (LOD) was calculated based on the generally accepted method the $\mathbf{LOD{=}3 \times s_{blank}/m}$, where the $\boldsymbol{s_{blank}}$ is the standard deviation of the blank signal, while $\boldsymbol{m}$ is the slope of the initial range of calibration curve [49]. The smallest detectable amount of Vitamin B_2 is 2.01 ± 0.31 μM.

Although, this value cannot be comparable with the limit of detection in the case of large instrument techniques (Fig S6 and Table 1), the determined 2.01 ± 0.31 μM value is suitable to develop some fast optical sensors for food samples. The fluorescence quenching was analyzed in the large 2.0–1000 μM concentration range of B_2. The usable range of

Table 1
Identification of Vitamin B_2 (riboflavin) by different techniques.

Technique/Material	Detection or Measuring limit	Sample type	Ref.
Liquid chromatography	2.1–871 μg g^{-1}	foods	[50]
Liquid chromatography	0.3–50 μg g^{-1}	foods	[51]
Biacore® Q biosensor	100–500 μg/100 g	aqueous solution	[52]
Adenosine-stabilized gold nanoclusters	0.002 nM	cell fluid by fluorescence quenching	[47]
quinoline-pyridine-combined chemosensor modified by tetraphenylethene and chelating with Cd^{2+}	70.52 nM	in aqueous solution by fluorescence enhancement and shift from green (550 nm) to blue (475 nm)	[53]
Thionine Coated Cadmium Selenide Quantum Dots Modified Graphite Electrode	53 × 10^{-9} M	in aqueous solution by voltametric detection	[54]
amperometric detection of riboflavin	0.85 nM	amperometric detection	[55]
Fe_3O_4/rGO hybrid nanocomposites	no data	electrochemical detection of riboflavin	[56]

the liquid sensor system was pointed out between 2.5–500.0 μM (Fig S7A) by the polynomial fitting of the relative fluorescence (I_0/I) as a function of Vitamin B_2 concentration (Fig. S7B). A possible application of the prepared AMP-Cu NCs is as a fluorescent assay for the detection of Vitamin B_2 molecule. We performed the analysis of complex food and pharmaceutical samples, where a casual nutritional yeast and two types of dietary supplement were selected. Before the analysis, the samples were powdered and dissolved into mildly alkaline sodium chloride solutions (c = 0.15 M; pH=8.0). As can be seen in Table 2, the detected amounts are close to the expected B_2 concentrations.

The Recovery %, which refers to the accuracy of the developed fluorometric assay, was calculated by Eq. (4):

$$Recovery\% = \frac{Detectedamount}{Expectedamount} * 100 \quad (4)$$

Nevertheless, the experienced minimal differences between the measured and expected values can be considered the characteristics of the samples according to the opinion of the factories, Besides, it can belong to the sampling matrix containing 15 individual samples. However, the repetition error of the fluorometric assay was below 3 % for all measurements in the case of the same sample.

4. Conclusion

In this work, we demonstrated a novel synthesis route to produce AMP-stabilized Cu NCs. We identified the synthesis conditions where the best fluorescence intensity could be achieved for these systems. The prepared Cu_{13} NCs having blue fluorescence was thoroughly characterized. The optical measurements clearly showed that the formed particles had a cluster-type structure with *ca.* 1.8 % QY. The lack of satellites on the XP spectrum of the Cu proved the presence of metallic cores, which are stabilized by the adenine ring of AMP. The possible sensor applications for Vitamin B molecules were identified. The change in the chemical composition of AMP-stabilized cluster core from bimetallic Au/Ag to monometallic Cu caused the tuning of the selectivity from folic acid to riboflavin. The LOD value was *ca.* 2 μM, while the usability concentration range between 2.5–500 μM was also determined. The quenching mechanism is dominantly dynamic by the TCSPC measurements, and a charge/resonance energy transfer were proven by different techniques. Besides the possible application in the case of real word samples, which contains yeast or pills, are also presented.

5. Future perspectives

As presented in the Introduction, the possible sensor applications of novel fluorescent nanometals gained significant scientific interest recently. The quick analysis of food industrial or pharmaceutical samples is especially important task to guarantee uniform quality products (*e.g.* identification of fake wine). For these purposes, developing cheap, selective, and sensitive tests, which are easily used, is in exceptionally high demand. The possible application of AMP-Cu NCs for detecting Vitamin B_2 can be eco-friendly and cost-effective to solve these requirements and challenges. Therefore, the presented work offers a promising alternative for the analysis of complex samples such as food industrial yeast, which is an essential basic material for bakery and beer production. In addition, it provides even smaller companies with the opportunity to perform/develop rapid tests for the diagnosis of vitamins and dietary supplements without having to expensive and specialized instruments.

Funding

The research was supported by the National Research, Development, and Innovation Office-NKFIH through the PD137938 project. Ditta Ungor thanks the financial support for the János Bolyai Research Scholarship of the Hungarian Academy of Sciences. This paper was supported by the ÚNKP-23-5-SZTE-670 New Excellence Program of The Ministry for Culture and Innovation from the Source of The National Research, Development and Innovation Fund.

Table 2
The expected and measured amount of Vitamin B_2 in real samples (n = 5, average values presented).

Sample		Detected (μM)	Expected (μM)[1]	Recovery %
I.	pill 1	6.72	6.64	101
	pill 2	5.93		89
	pill 3	7.05		106
II.	pill 1	82.5	74.4	111
	pill 2	70.6		95
	pill 3	73.8		99
III.	yeast 1	8.29	*ca.* 7.97	104
	yeast 2	7.99		101
	yeast 3	8.06		102

I. pill: 2.5 mg B_2/pill in *B-complex + folic acid* produced by JuvaPharma, Hungary, Káva.
II. pill: 28 mg B_2/pill in *B_2 Vitamin – Riboflavin* produced by GymBeam, Hungary, Budapes.
III. yeast: Hungarian *yeast of Budafok* produced by Lessafre Hungary, Budapest.
[1]The expected amount was calculated based on the preparation protocols of the samples and the riboflavin content provided by the manufacturers.

CRediT authorship contribution statement

Ditta Ungor: Writing – original draft, Visualization, Methodology, Investigation, Funding acquisition, Data curation, Conceptualization. **Loretta Kuklis:** Methodology, Investigation. **Gergely F. Samu:** Writing – review & editing, Visualization, Investigation. **Edit Csapó:** Writing – review & editing.

Declaration of competing interest

The authors declare that they have no known competing financial interests or personal relationships that could have appeared to influence the work reported in this paper.

Data availability

Data will be made available on request.

Appendix A. Supplementary data

Supplementary data to this article can be found online at https://doi.org/10.1016/j.microc.2024.111257.

References

[1] Y. Wang, M. Lu, D. Tang, Novel photoluminescence enzyme immunoassay based on supramolecular host-guest recognition using L-arginine/6-aza-2-thiothymine-stabilized gold nanocluster, Biosens. Bioelectron. 109 (2018) 70–74, https://doi.org/10.1016/j.bios.2018.03.007.
[2] Y. An, Y. Ren, M. Bick, A. Dudek, E. Hong-Wang Waworuntu, J. Tang, J. Chen, B. Chang, Highly fluorescent copper nanoclusters for sensing and bioimaging, Biosens. Bioelectron. 154 (2020) 112078, https://doi.org/10.1016/j.bios.2020.112078.
[3] J. Ma, Z. Lu, C. Li, Y. Luo, Y. Shi, P. Alam, J.W.Y. Lam, Z. Wang, B.Z. Tang, Fluorescence ratiometric assay for discriminating GSH and Cys based on the composites of UiO-66-NH2 and Cu nanoclusters, Biosens. Bioelectron. 215 (2022) 114582, https://doi.org/10.1016/j.bios.2022.114582.
[4] J. Zheng, C. Zhou, M. Yu, J. Liu, Different sized luminescent gold nanoparticles, Nanoscale 4 (2012) 4073, https://doi.org/10.1039/c2nr31192e.
[5] Z. Cai, L. Wu, K. Qi, C. Deng, C. Zhang, Blue-emitting glutathione-capped copper nanoclusters as fluorescent probes for the highly specific biosensing of furazolidone, Spectrochim. Acta A Mol. Biomol. Spectrosc. 247 (2021) 119145, https://doi.org/10.1016/j.saa.2020.119145.
[6] D. Ungor, I. Dékány, E. Csapó, Reduction of Tetrachloroaurate(III) Ions With Bioligands: Role of the Thiol and Amine Functional Groups on the Structure and

Optical Features of Gold Nanohybrid Systems, Nanomaterials 9 (2019) 1229, https://doi.org/10.3390/nano9091229.
[7] X. Gao, Z. Ma, M. Sun, X. Liu, K. Zhong, L. Tang, X. Li, J. Li, A highly sensitive ratiometric fluorescent sensor for copper ions and cadmium ions in scallops based on nitrogen doped graphene quantum dots cooperating with gold nanoclusters, Food Chem. 369 (2022) 130964, https://doi.org/10.1016/j.foodchem.2021.130964.
[8] X. Yue, Q. Pan, J. Zhou, H. Ren, C. Peng, Z. Wang, Y. Zhang, A simplified fluorescent lateral flow assay for melamine based on aggregation induced emission of gold nanoclusters, Food Chem. 385 (2022) 132670, https://doi.org/10.1016/j.foodchem.2022.132670.
[9] L. Wang, W. Wang, L. Zhang, J. Li, J. Sun, S. Wang, X. Mao, Simultaneous screening of multiple diarrhetic shellfish poisons with group-specific split aptamers and silver nanocluster beacon, Food Chem. 410 (2023) 135389, https://doi.org/10.1016/j.foodchem.2023.135389.
[10] Y. Yang, B. Ghalandari, L. Lin, X. Sang, W. Su, A. Divsalar, X. Ding, A turn-on fluorescence sensor based on Cu2+ modulated DNA-templated silver nanoclusters for glyphosate detection and mechanism investigation, Food Chem. 367 (2022) 130617, https://doi.org/10.1016/j.foodchem.2021.130617.
[11] Y. Ma, H. Mei, Y. Li, P. Zhou, G. Mao, H. Wang, X. Wang, A novel raiometric fluorescence probe based on silicon quantum dots and copper nanoclusters for visual assay of l-cysteine in milks, Food Chem. 379 (2022) 132155, https://doi.org/10.1016/j.foodchem.2022.132155.
[12] S. Mashhadi Farahani, M. Dadmehr, M. Ali Karimi, B. Korouzhdehi, M. Amin Karimi, M. Rajabian, Fluorometric detection of phytase enzyme activity and phosphate ion based on gelatin supported silver nanoclusters, Food Chem. 396 (2022) 133711, https://doi.org/10.1016/j.foodchem.2022.133711.
[13] Y. Lei, Y. Zhang, L. Yuan, J. Li, Biochar-supported Cu nanocluster as an electrochemical ultrasensitive interface for ractopamine sensing, Food Chem. X 15 (2022) 100404, https://doi.org/10.1016/j.fochx.2022.100404.
[14] Y. Shi, W. Li, X. Feng, L. Lin, P. Nie, J. Shi, X. Zou, Y. He, Sensing of mercury ions in Porphyra by Copper @ Gold nanoclusters based ratiometric fluorescent aptasensor, Food Chem. 344 (2021) 128694, https://doi.org/10.1016/j.foodchem.2020.128694.
[15] L. Chen, J. Lu, M. Luo, H. Yu, X. Chen, J. Deng, X. Hou, E. Hao, J. Wei, P. Li, A ratiometric fluorescent sensing system for the selective and ultrasensitive detection of pesticide residues via the synergetic effects of copper nanoclusters and carbon quantum dots, Food Chem. 379 (2022) 132139, https://doi.org/10.1016/j.foodchem.2022.132139.
[16] B. Hemmateenejad, F. Shakerizadeh-Shirazi, F. Samari, BSA-modified gold nanoclusters for sensing of folic acid, Sens Actuators B Chem 199 (2014) 42–46, https://doi.org/10.1016/j.snb.2014.03.075.
[17] J. Liu, L. Gan, X. Yang, Glutenin-directed gold nanoclusters employed for assaying vitamin B1, New J. Chem. 44 (2019) 487–491, https://doi.org/10.1039/c9nj04570h.
[18] Z. Li, T. Zhang, M. Zhang, W. Hu, Detection of folic acid and imaging of folate receptor overexpressed cancer cells via a far-red silver nanoclusters with Baseline Resolved Between Excitation and Emission, Dyes Pigm. 198 (2022) 109984, https://doi.org/10.1016/j.dyepig.2021.109984.
[19] Y. Luo, H. Miao, X. Yang, Glutathione-stabilized Cu nanoclusters as fluorescent probes for sensing pH and vitamin B1, Talanta 144 (2015) 488–495, https://doi.org/10.1016/j.talanta.2015.07.001.
[20] K. Yang, Y. Wang, C. Lu, X. Yang, Ovalbumin-directed synthesis of fluorescent copper nanoclusters for sensing both vitamin B1 and doxycycline, J. Lumin. 196 (2018) 181–186, https://doi.org/10.1016/j.jlumin.2017.12.038.
[21] D. Ungor, I. Szilágyi, E. Csapó, Yellow-emitting Au/Ag bimetallic nanoclusters with high photostability for detection of folic acid, J. Mol. Liq. 338 (2021) 116695, https://doi.org/10.1016/j.molliq.2021.116695.
[22] A. Lopez, J. Liu, Light-activated metal-coordinated supramolecular complexes with charge-directed self-assembly, J. Phys. Chem. C 117 (2013) 3653–3661, https://doi.org/10.1021/jp3121403.
[23] J. Liu, DNA-stabilized, fluorescent, metal nanoclusters for biosensor development, TrAC - Trends Anal. Chem. 58 (2014) 99–111, https://doi.org/10.1016/j.trac.2013.12.014.
[24] C.-X. Zhang, Y.-C. Gao, C. Wang, X. Yu, H.-W. Li, Y. Wu, Aggregation-induced emission enhancement of adenosine monophosphate-capped bimetallic nanoclusters by aluminum(III) ions, and its application to the fluorometric determination of cysteine, Microchim. Acta 187 (2020) 41, https://doi.org/10.1007/s00604-019-3901-z.
[25] S. Jeong, K. Woo, D. Kim, S. Lim, J.S. Kim, H. Shin, Y. Xia, J. Moon, Controlling the Thickness of the Surface Oxide Layer on Cu Nanoparticles for the Fabrication of Conductive Structures by Ink-Jet Printing, Adv. Funct. Mater. 18 (2008) 679–686, https://doi.org/10.1002/adfm.200700902.
[26] Y.Z. Lu, W.T. Wei, W. Chen, Copper nanoclusters: synthesis, characterization and properties, Chin. Sci. Bull. 57 (2012) 41–47, https://doi.org/10.1007/s11434-011-4896-y.
[27] A. Baghdasaryan, T. Bürgi, Copper nanoclusters: designed synthesis, structural diversity, and multiplatform applications, Nanoscale 13 (2021) 6283–6340, https://doi.org/10.1039/d0nr08489a.
[28] M. Cui, G. Song, C. Wang, Q. Song, Synthesis of cysteine-functionalized water-soluble luminescent copper nanoclusters and their application to the determination of chromium(VI), Microchim. Acta 182 (2015) 1371–1377, https://doi.org/10.1007/s00604-015-1458-z.
[29] B. Han, T. Peng, Y. Li, M. Yu, X. Hu, G. He, Ultra-stable L-proline protected copper nanoclusters and their solvent effect, Methods Appl Fluoresc 6 (2018), https://doi.org/10.1088/2050-6120/aac8f5.
[30] V.A. Sadhu, S. Jha, T.J. Park, S.K. Kailasa, Synthesis of copper nanoclusters from Bacopa monnieri leaves for fluorescence sensing of dichlorvos, Luminescence 38 (2023) 1872–1882, https://doi.org/10.1002/bio.4575.
[31] Harshita, T.J. Park, S.K. Kailasa, Microwave-assisted synthesis of green fluorescent copper nanoclusters: a novel approach for sensing of hydroxyl radicals and pyrophosphate ions via a "turn-off–on" mechanism, New J. Chem. 47 (2023) 20038–20047, https://doi.org/10.1039/D3NJ03751G.
[32] J.B. Raval, V.N. Mehta, S. Jha, T.J. Park, S.K. Kailasa, Biosynthesis of Green-Emissive Copper Nanoclusters from Plectranthus scutellarioides Extract for the Detection of Terbufos in Carrot and Water Samples, ACS Food Sci. Technol. 4 (2024) 272–281, https://doi.org/10.1021/acsfoodscitech.3c00539.
[33] D. Ungor, E. Csapó, B. Kismárton, A. Juhász, I. Dékány, Nucleotide-directed syntheses of gold nanohybrid systems with structure-dependent optical features: Selective fluorescence sensing of Fe3+ ions, Colloids Surf. B Biointerfaces 155 (2017) 135–141, https://doi.org/10.1016/j.colsurfb.2017.04.013.
[34] N.K. Das, S. Ghosh, A. Priya, S. Datta, S. Mukherjee, Luminescent Copper Nanoclusters as a Specific Cell-Imaging Probe and a Selective Metal Ion Sensor, J. Phys. Chem. C 119 (2015) 24657–24664, https://doi.org/10.1021/acs.jpcc.5b08123.
[35] P.F. Lang, Fermi energy, metals and the drift velocity of electrons, Chem. Phys. Lett. 770 (2021) 138447, https://doi.org/10.1016/j.cplett.2021.138447.
[36] Y. Jia, Z. Luo, Thirteen-atom metal clusters for genetic materials, Coord. Chem. Rev. 400 (2019) 213053, https://doi.org/10.1016/j.ccr.2019.213053.
[37] M. Lettieri, P. Palladino, S. Scarano, M. Minunni, Copper nanoclusters and their application for innovative fluorescent detection strategies: an overview, Sens. Actuators Rep. 4 (2022) 100108, https://doi.org/10.1016/j.snr.2022.100108.
[38] G. Pétaud, F. Gaillard, M. Tayakout, S. Gil, A. Giroir-Fendler, Spotlight on Large Surface Copper Cluster Role of Cu-SAPO-34 Catalyst in Standard NH3-SCR Performances, ChemCatChem 12 (2020) 2807–2822, https://doi.org/10.1002/cctc.201902036.
[39] S. Peters, S. Peredkov, M. Al-Hada, M. Neeb, W. Eberhardt, Positive XPS binding energy shift of supported CuN-clusters governed by initial state effects, J Electron. Spectros. Relat. Phenomena 192 (2014) 52–54, https://doi.org/10.1016/j.elspec.2014.01.011.
[40] M. Swadźba-Kwaśny, L. Chancelier, S. Ng, H.G. Manyar, C. Hardacre, P. Nockemann, Facile in situ synthesis of nanofluids based on ionic liquids and copper oxide clusters and nanoparticles, Dalton Trans. 41 (2012) 219–227, https://doi.org/10.1039/c1dt11578b.
[41] J.P. Vanegas, E. Zaballos-García, M. González-Béjar, P. Londoño-Larrea, J. Pérez-Prieto, Adenosine monophosphate-capped gold(I) nanoclusters: Synthesis and lanthanide ion-induced enhancement of their luminescence, RSC Adv. 6 (2016) 17678–17682, https://doi.org/10.1039/c6ra01891b.
[42] M. Furukawa, T. Yamada, S. Katano, M. Kawai, H. Ogasawara, A. Nilsson, Geometrical characterization of adenine and guanine on Cu(1 1 0) by NEXAFS, XPS, and DFT calculation, Surf. Sci. 601 (2007) 5433–5440, https://doi.org/10.1016/j.susc.2007.09.009.
[43] H.A. Tajmir-Riahi, T. Theophanides, Adenosine-5′-monophosphate complexes of Pt (II) and Mg(II) metal ions. Synthesis, FTIR Spectra and Structural Studies, Inorg. Chim. Acta 80 (1983) 183–190, https://doi.org/10.1016/S0020-1693(00)91280-5.
[44] S. Jin, W. Liu, D. Hu, X. Zou, X. Kang, W. Du, S. Chen, S. Wei, S. Wang, M. Zhu, Aggregation-Induced Emission (AIE) in Ag−Au Bimetallic Nanocluster, Chem. A Eur. J. 24 (2018) 3712–3715, https://doi.org/10.1002/chem.201800189.
[45] V. Leandri, Q. Daniel, H. Chen, L. Sun, J.M. Gardner, L. Kloo, Electronic and Structural Effects of Inner Sphere Coordination of Chloride to a Homoleptic Copper (II) Diimine Complex, Inorg. Chem. 57 (2018) 4556–4562, https://doi.org/10.1021/acs.inorgchem.8b00225.
[46] A. Aracena, M.C. Rezende, M. García, K. Muñoz-Becerra, K. Wrighton-Araneda, C. Valdebenito, F. Celis, O. Vásquez, Alkylated Benzodithienoquinolizinium Salts as Possible Non-Fullerene Organic N-Type Semiconductors: An Experimental and Theoretical Study, Materials 14 (2021) 6239, https://doi.org/10.3390/ma14216239.
[47] C. Zeng, Y. Mu, W. Cao, Q. Zhuang, Y. Wang, Water-Soluble Photoluminescent Adenosine-Functionalized Gold Nanoclusters as Highly Sensitive and Selective Receptors for Riboflavin Detection in Rat Brain, Anal. Chem. 95 (2023) 1671–1679, https://doi.org/10.1021/acs.analchem.2c04803.
[48] S.L.J. Tan, R.D. Webster, Electrochemically Induced Chemically Reversible Proton-Coupled Electron Transfer Reactions of Riboflavin (Vitamin B 2), J. Am. Chem. Soc. 134 (2012) 5954–5964, https://doi.org/10.1021/ja300191u.
[49] E. Akyüz, F.B. Şen, M. Bener, K.S. Başkan, E. Tütem, R. Apak, Protein-Protected Gold Nanocluster-Based Biosensor for Determining the Prooxidant Activity of Natural Antioxidant Compounds, ACS Omega 4 (2019) 2455–2462, https://doi.org/10.1021/acsomega.8b03286.
[50] F. Arella, S. Lahély, J.B. Bourguignon, C. Hasselmann, Liquid chromatographic determination of vitamins B1 and B2 in foods. A Collaborative Study, Food Chem. 56 (1996) 81–86, https://doi.org/10.1016/0308-8146(95)00149-2.
[51] S. Ndaw, M. Bergaentzlé, D. Aoudé-Werner, C. Hasselmann, Extraction procedures for the liquid chromatographic determination of thiamin, riboflavin and vitamin B6 in foodstuffs, Food Chem. 71 (2000) 129–138, https://doi.org/10.1016/S0308-8146(00)00135-7.
[52] Y. Gao, F. Guo, S. Gokavi, A. Chow, Q. Sheng, M. Guo, Quantification of water-soluble vitamins in milk-based infant formulae using biosensor-based assays, Food Chem. 110 (2008) 769–776, https://doi.org/10.1016/J.FOODCHEM.2008.03.007.
[53] H. Xie, M. Zhou, X. Cui, C. Li, Y. Wu, X. Luo, M. Sen Yuan, A metal-complex based chemosensor for the detection of riboflavin and folate, Spectrochim Acta A Mol

Biomol Spectrosc 304 (2024) 123321. https://doi.org/10.1016/J.SAA.2023.123321.

[54] R.A. Puglisi, J. Adam, R. Duffy, A. Kalaivani, R. Suresh Babu, S.S. Narayanan, Highly Sensitive Sensor for the Determination of Riboflavin Using Thionine Coated Cadmium Selenide Quantum Dots Modified Graphite Electrode, Micro 2023, Vol. 3, Pages 686-698 3 (2023) 686–698. https://doi.org/10.3390/MICRO3030048.

[55] Y.Y. Yu, J.X. Wang, R.W. Si, Y. Yang, C.L. Zhang, Y.C. Yong, Sensitive amperometric detection of riboflavin with a whole-cell electrochemical sensor, Anal. Chim. Acta 985 (2017) 148–154, https://doi.org/10.1016/J.ACA.2017.06.053.

[56] R. Madhuvilakku, S. Alagar, R. Mariappan, S. Piraman, Green one-pot synthesis of flowers-like Fe3O4/rGO hybrid nanocomposites for effective electrochemical detection of riboflavin and low-cost supercapacitor applications, Sens Actuators B Chem 253 (2017) 879–892, https://doi.org/10.1016/J.SNB.2017.06.126.